Plasma Astrophysics

Toshiki Tajima, UCI

Class 3:PHY249 (2020Spring)

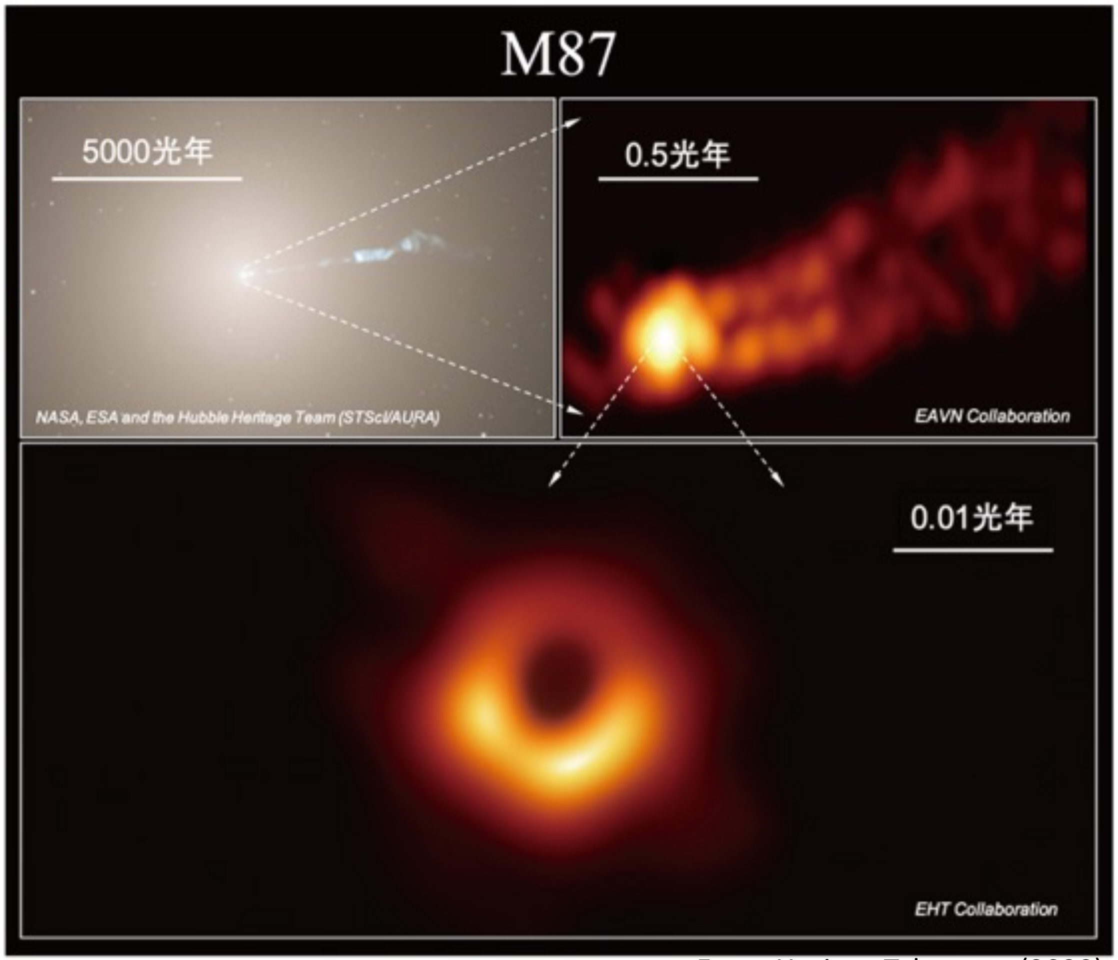

Event Horizon Telescope (2020)

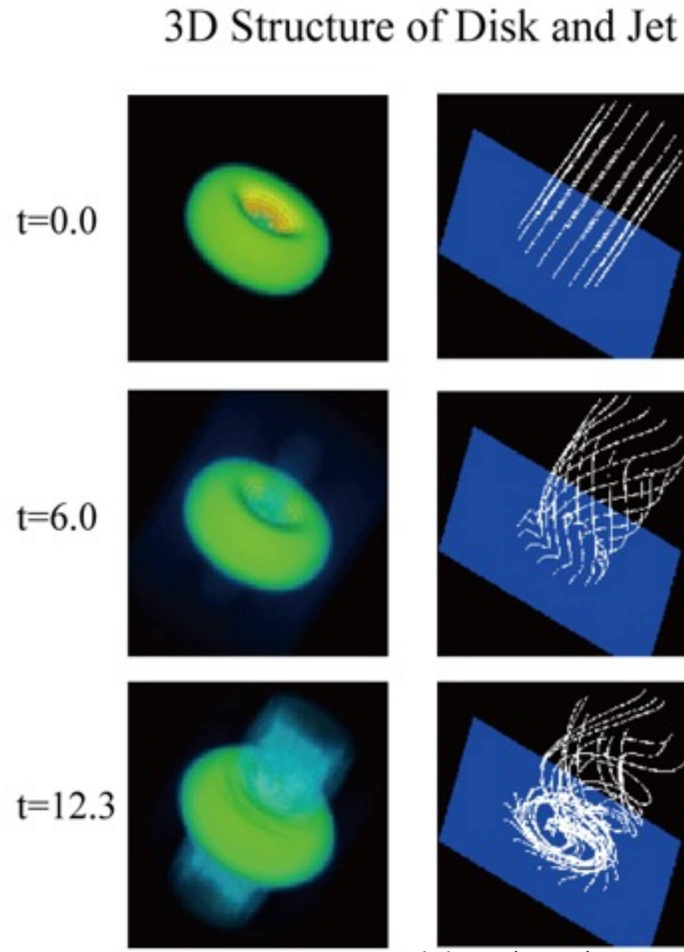

Tajima Shibata (1997) p. 387

Filamentary **plasma**

ig. II.10. Contrast-enhanced photograph of the Orion nebula (*Sky and Telescope*, April, 1979).

ect. None of the observed filaments can be regarded with any certainty as resulting
m such effects, whereas in all cases there is either convincing proof, or reasonably

H. Alfven (1981) "Cosmic Plasma"

What are the ingredients?

- gravity
- plasma
- B

to make a spaghetti plasma

Can you also point out other filamentary plasma pictures in the textbook (1997)?

Can you tell what in each picture made them filamentary?

What part of astrophysics?

- Frontiers of astrophysics only (that are not yet well understood):

  highest energy particles (e.g. of cosmic rays > 10^20eV, high energy neutrinos)

  highest energy photons (e.g. γ-rays up to TeV /PeV)

  most violent processes (e.g. disruptive accretion; jets)

  episodic and eruptive (e. g. γ-ray bursts)

  young objects (e. g. AGN, Blazars, colliding galaxies (M82), microquasars (SS433),…)

  neutron-star x neutron-star collision→ plasma plays essential role

  ……….

- I have no time to cover:

  old objects (e.g. our galaxy, our Sun, our solar system), gravitational dominants

  quiet, steady-state objects

  objects where little plasma such as the Moon ("the older, the less plasma")

  single particle interacts with astronomical object (cf. collective interaction N^2)

  ………..

(our textbook covers some of both kinds)

Distinction between gravity ←→ EM

- Both: range can be **infinite** ← Gauss law
- Strong and weak interactions:

  → range O(fermi = fm)

- Grav: **no** negative mass; EM: + and **–,** but can be combined;

  no magnetic monopole ➔ magnetic force range finite

- EM: if combined +/- → atoms : range O(Å)
- EM: +/- → Debeye screening: range O(v_t/ω_p)

  → collisionless skindepth: range O(c/ω_p)

  → EM radiation infinite range

However,

- With B : fields screening **removed** ← **Alfven** effect

  mediated @ $\boldsymbol{v_A}$

  : **texture** appears

- **Collective**/ violent proc. → ephemeral struct. or

  → robust struct = **wake** @ $\boldsymbol{c}$

Examples of base processes

Parker **instability**
(ballooning instability) → **Flux buoyancy**

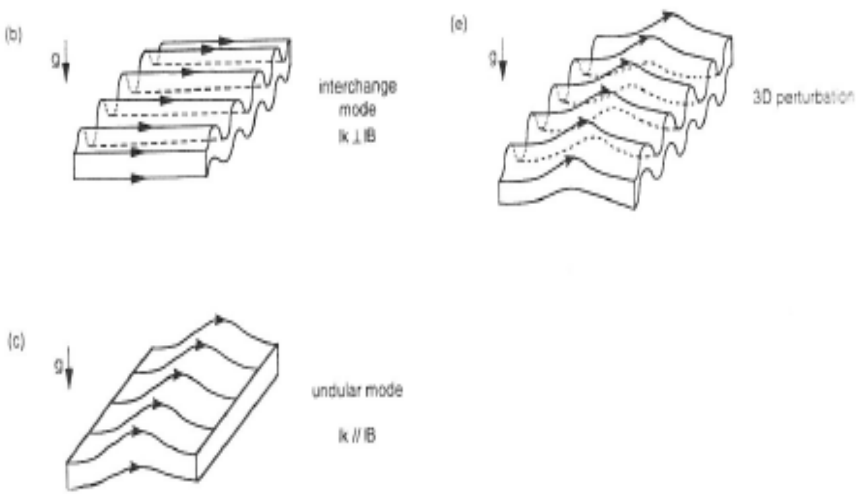

FIGURE 3.18 Interchange mode and undular (Parker) mode of magnetic buoyancy instability.

3.2.1.2 Magnetic Buoyancy Instability and Parker Instability

MRI → **twisted magnetic amplification; jet formation**

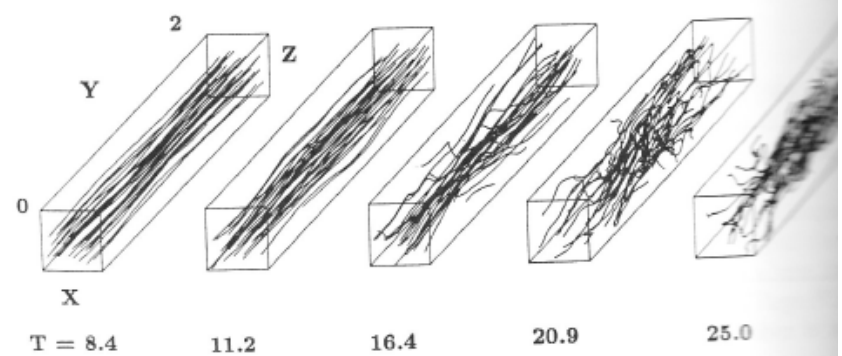

FIGURE 4.27 Magnetic field lines for model T in the eigenmode growth state $[t = (8.4 - 16.4$ ... saturation stage $[t = (20.9 - 25.0/\Omega]$ (Matsumoto and Tajima, 1995).

4.2.3.6 Effects of the Parker Instability*

When the vertical gravity is included, magnetic field escapes from the disk ... due to the Parker instability (the magneto-buoyancy instability; see Sec. ... growth rate of the Parker instability is $2 - 5H/v_A$, the growth rate of the Parker ... becomes comparable to that of the magnetic shearing instability as β approaches ...

Text p.158-196

Text p. 329-342

Nonlinear evolution of Parker Instability

Collaboration of gravity and plasma + B → nonlinear evolution (can be explosive*)

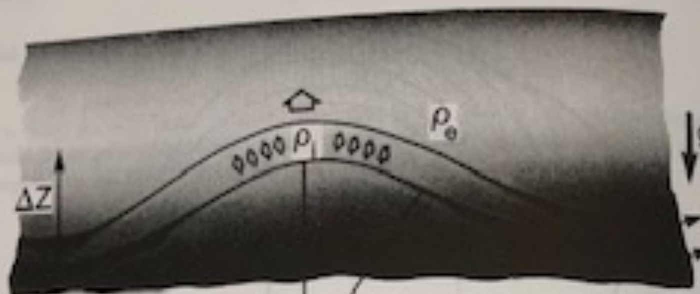

Mass falls off along the flux tube
→ Stimulate further growth of balloon
→ "overshoot"

FIGURE 3.20 Undulating flux tube (or sheet).

as shown before (Eq. 3.2.4). Since the magnetic tension force is of order of $B^2/(4\pi\lambda)$, the instability condition becomes

$$\lambda > 2H. \qquad (3.2.34)$$

Consequently, there is a critical wavelength below which the Parker mode is stable and the critical wavelength is of order of the local pressure scale height. As discussed earlier, above isothermal isolated flux tube is not in equilibrium, and hence these calculations are not exact (buoyancy force is too large).

Now consider a flux sheet in equilibrium and assume that both sound speed C_s and Alfvén speed V_A are constant. The unperturbed state of plasmas and magnetic field are given by the following equations,

$$p/p_0 = \rho/\rho_0 = B^2/B_0^2 = \exp(-z/\Lambda), \qquad (3.2.35)$$

where

(3.2.36)

... obtained from a hydrostatic balance along the flux tube (sheet) and there is no magnetic force along the flux tube, the density at the top of the raised portion of the tube becomes

$$\rho_i(\Delta z) \simeq \rho_0 \exp(-\Delta z/H) \simeq \rho_0(1 - \Delta z/H), \qquad (3.2.37)$$

where

$$H = C_s^2/g. \qquad (3.2.38)$$

On the other hand, the density outside the tube (sheet) at the same height (Δz) is

$$\rho_e(\Delta z) \simeq \rho_0 \exp(-\Delta z/\Lambda) \simeq \rho_0(1 - \Delta z/\Lambda). \qquad (3.2.39)$$

Hence, the net density depression at the top of the loop is

$$\Delta\rho \simeq \rho_e(\Delta z) - \rho_i(\Delta z) \simeq \rho_0 \Delta z\left(\frac{1}{H} - \frac{1}{\Lambda}\right). \qquad (3.2.40)$$

The curvature radius r is rewritten using the wavelength λ as

$$r \simeq \left(\frac{\lambda}{4}\right)^2 \frac{2}{\Delta z}. \qquad (3.2.41)$$

Then after some manipulation, the condition for occurrence of the Parker instability $\Delta\rho g > B^2/4\pi r$ becomes

$$\lambda^2 > \lambda_c^2 = 16\Lambda^2/(1 + 1/\beta), \qquad (3.2.42)$$

where β is the ratio of gas pressure to magnetic pressure.

Finally the instability condition for wavelength becomes

$$\lambda > \lambda_c = 4\Lambda/(1 + 1/\beta)^{1/2}. \qquad (3.2.43)$$

An exact treatment (Parker, 1966, 1979) shows the dispersion relation for $k_y\Lambda \gg 1$ as follows

$$(2/\beta + \gamma)\Omega^4 + [(4/\beta)(1/\beta + \gamma)(k_x^2\Lambda^2 + 1/4) + \gamma - 1]\Omega^2$$
$$+ (2/\beta)k_x^2\Lambda^2[(2/\beta)\gamma k_x^2\Lambda^2 - (1 + 1/\beta)(1 + 1/\beta - \gamma)] = 0, \qquad (3.2.44)$$

where

$$\Omega = \frac{\omega\Lambda}{C_s} \qquad (3.2.45)$$

and y is the direction perpendicular to both vertical and magnetic fields. From this, we find the exact critical wavelength for $k_y\Lambda \gg 1, \gamma = 1$ as

*Explosive processes

- Cooperative process
- "vicious cycle" (or "rich gets richer process")
- $$da_1 / dt = \gamma\, a_2\, a_1 ,$$
  $$da_2 / dt = \gamma\, a_1\, a_2 .$$
  $$\rightarrow \quad a_{1,\,2} \sim 1 / (t_0 - t)^{\alpha}$$

explodes in finite time (t_0) to infinite amplitude

cf. $$da_1/dt = \gamma\, a_0\, a_1 - \beta\, a_1.$$

exponentiates if $a_0 > \beta/\gamma$

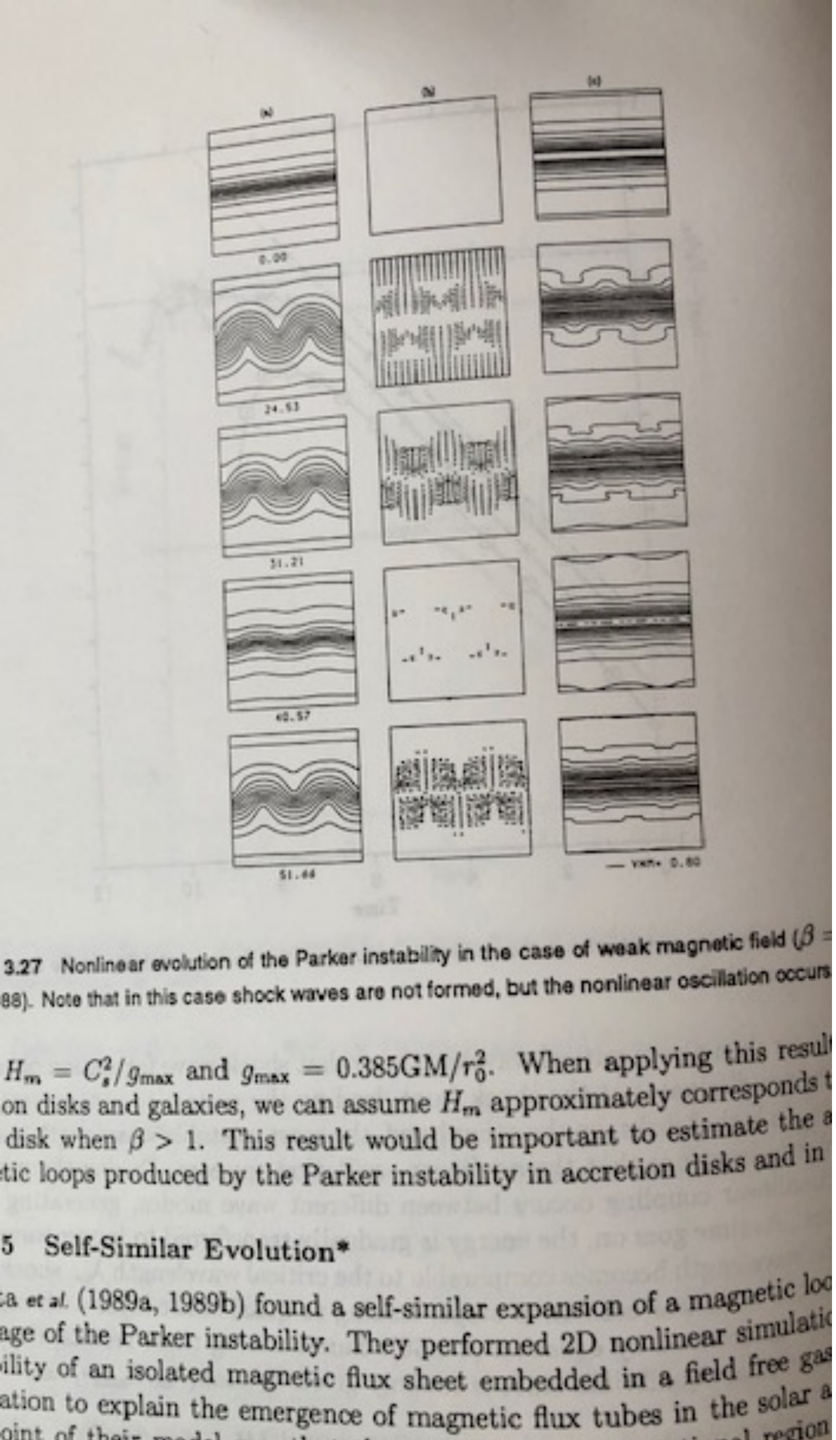

Beginning of **structure formation**

via Parker process

Consequences:

→ 1. the escape of amplified B-field in the disk

2. pinching of plasma radially accentuated, forming **streaks** of dense regions

3. allow accentuated magneto-rotational instability onset

4. assist jet formation

5. assist **accretion of clumped matter**

Magnetic buoyancy and twist in jets from accretion disk

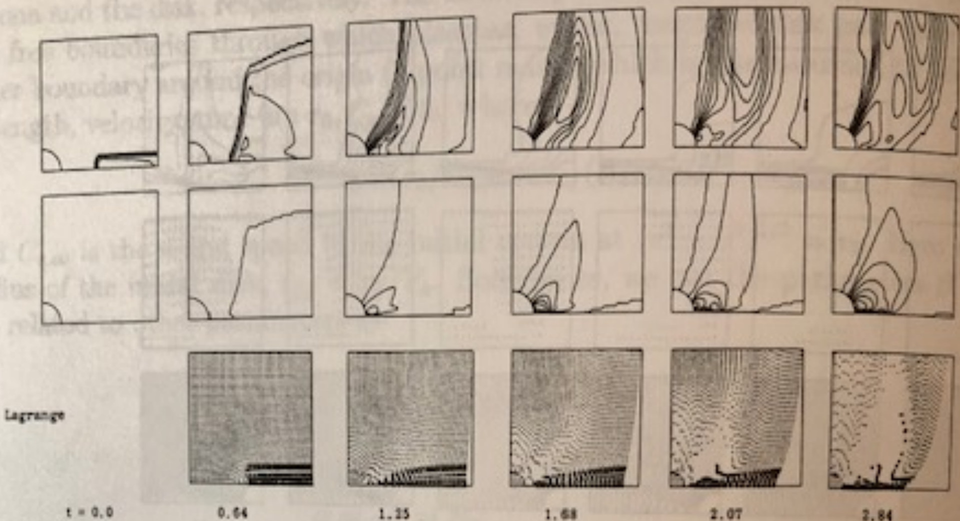

FIGURE 4.53 2.5D MHD sim. of magnetic twist jet (Shibata and Uchida, 1986a): v_φ, B_φ, Lagrange.

of jet.

Figure 4.55 shows the dependence on the plasma β. It is seen that the magneti more rigid in low $\beta(=0.3)$ case, while it is more undulating in high $\beta(=5)$ case. I found that the velocity of jet is higher in low β case than in high β case. Empirica is written as

$$V_{\rm jet} \sim \beta^{-0.3\sim-0.4} \sim B^{0.5\sim0.7}.$$

Interestingly, this relation is roughly in agreement with the relation of Michel's mi energy solution for a fast rotator (equation (4.3.35) in previous subsection). Accordin and Shibata (1986, unpublished), the low β jet is accelerated mainly by the centrifuga whereas the high β jet is by the magnetic pressure gradient force. The dependence initial rotational velocity is shown in Figure 4.56. From this, we find that even the i Keplerian case leads to contraction due to magnetic braking and hence eventually t though the velocity of the jet is slower than the sub-Keplerian case. More detailed comp between the jet formation and the Balbus-Hawley mchanism (or Velikhov-Chandras

380

A consequence of Parker process
But we need twist in addition.

Gravity + Plasma +B
→ Jet formation

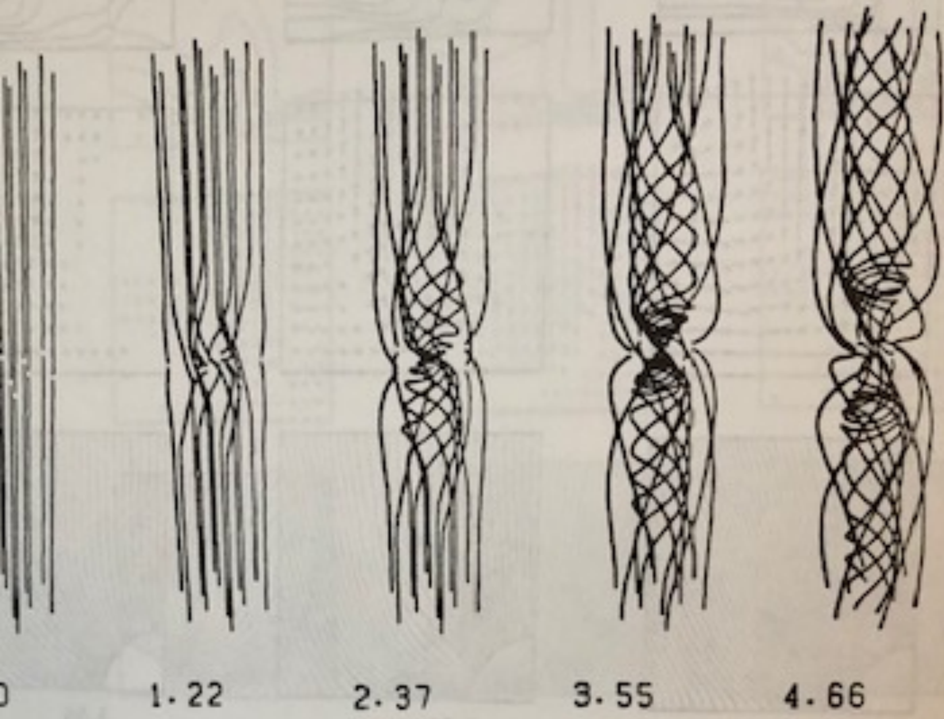
0 1.22 2.37 3.55 4.66

gnetic field configuration of *magnetic-twist* jet developed by Shibata and Uch

eady MHD Jets from Thick Disks*

p an AGN jet model, Matsumoto *et al.* (1996a) studied the cas
poloidal field, by performing nonsteady 2.5D MHD simulat
ida (1986a,b). (See Sec. 4.2.2.5.) Their results (see Fig. 4
tion) flow occurs along the surface of thick disks. (2) Magi
is and Hawley, 1991) occurs inside thick disks. (3) The v
ble to the Keplerian velocity, $V_{jet} \sim 0.6 - 2.3V_k \propto B^{0.15-}$
. (4) The mass loss rate by the jet $\dot{M}$ is in proportion to
. For the three-dimensional cases see Fig. 4.60.

ction between Stellar Magnetosphere and Accretion

buoyancy (not much angular momentum)

More global – twist (angular momentum)
→ jet

Extended structure of jets

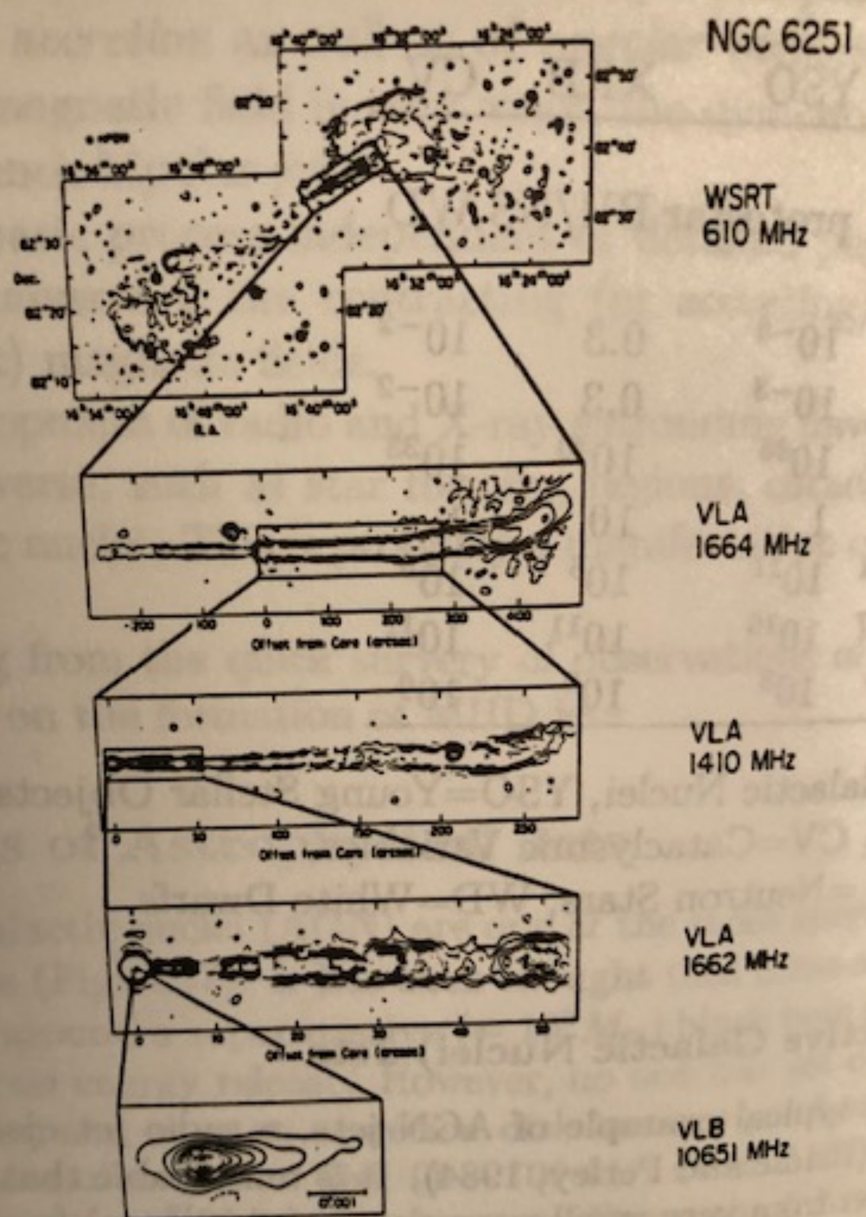

Radio images of jets ejected from nucleus of radio galaxy, NGC6251 (from Brid

Text p. 356

Jet (magnetically-driven flow):

and winds. The nonsteady MHD jet models will be discussed in Sec. 4.3.4.

1D Steady Magnetically Driven (Centrifugal) Wind

ensional, steady, centrifugal wind theory was developed by Weber and Davis (1967) a solar wind on the equatorial plane. Taking spherical coordinate (r, φ, θ), we eady state $\partial/\partial t = 0$, axisymmetry $\partial/\partial\varphi = 0$, no non-plane magnetic and velocity $\mathbf{B} = (B_r, B_\varphi, 0)$, $\mathbf{v} = (v_r, v_\varphi, 0)$), ideal (adiabatic) MHD, and 1D ($\partial/\partial\theta = 0$) on rial plane ($\theta = \pi/2$). Then, basic MHD equations are integrated into the following ation equations;

$$\rho v_r r^2 = f, \tag{4.3.9}$$

$$r^2 B_r = \Phi, \tag{4.3.10}$$

$$r\left(v_\varphi - \frac{B_r B_\varphi}{4\pi\rho v_r}\right) = \Omega r_A^2, \tag{4.3.11}$$

$$r(v_r B_\varphi - v_\varphi B_r) = -\Omega r^2 B_r, \tag{4.3.12}$$

$$p = K\rho^\gamma, \tag{4.3.13}$$

$$\frac{1}{2}v_r^2 + \frac{1}{2}(v_\varphi - \Omega r)^2 + \frac{\gamma}{\gamma-1}\frac{p}{\rho} - \frac{GM}{r} - \frac{\Omega^2 r^2}{2} = E. \tag{4.3.14}$$

he mass flux, Φ is the magnetic flux, Ω is the angular velocity of the Sun (or star ting body) from which wind or jet comes out, r_A is the Alfvén radius (discussed a constant depending only on entropy, and E is the total energy of the wind arameters f, Φ, Ω, r_A^2, K, E are integral constants. The unknown variables are $v_r, B_r, v_\varphi, B_\varphi$, and p. Hence, if these six constants are given, the equations are hat six unknown physical quantities are determined at each r.

ting v_φ in equations (4.3.11) and (4.3.12), we find

(4.3.15)

we obtain

Hence the de

Let us now

Eliminating

using other e

$H(r$

where

Since the equ

Hence the poi

obtain

Here

steady-state solution

<u>Bernoulli Eq.</u>

energy E = const

of gravity

potential ψ

angular freq Ω

(along the stream line)

(p. 364)

Jets from BH and magnetic fields

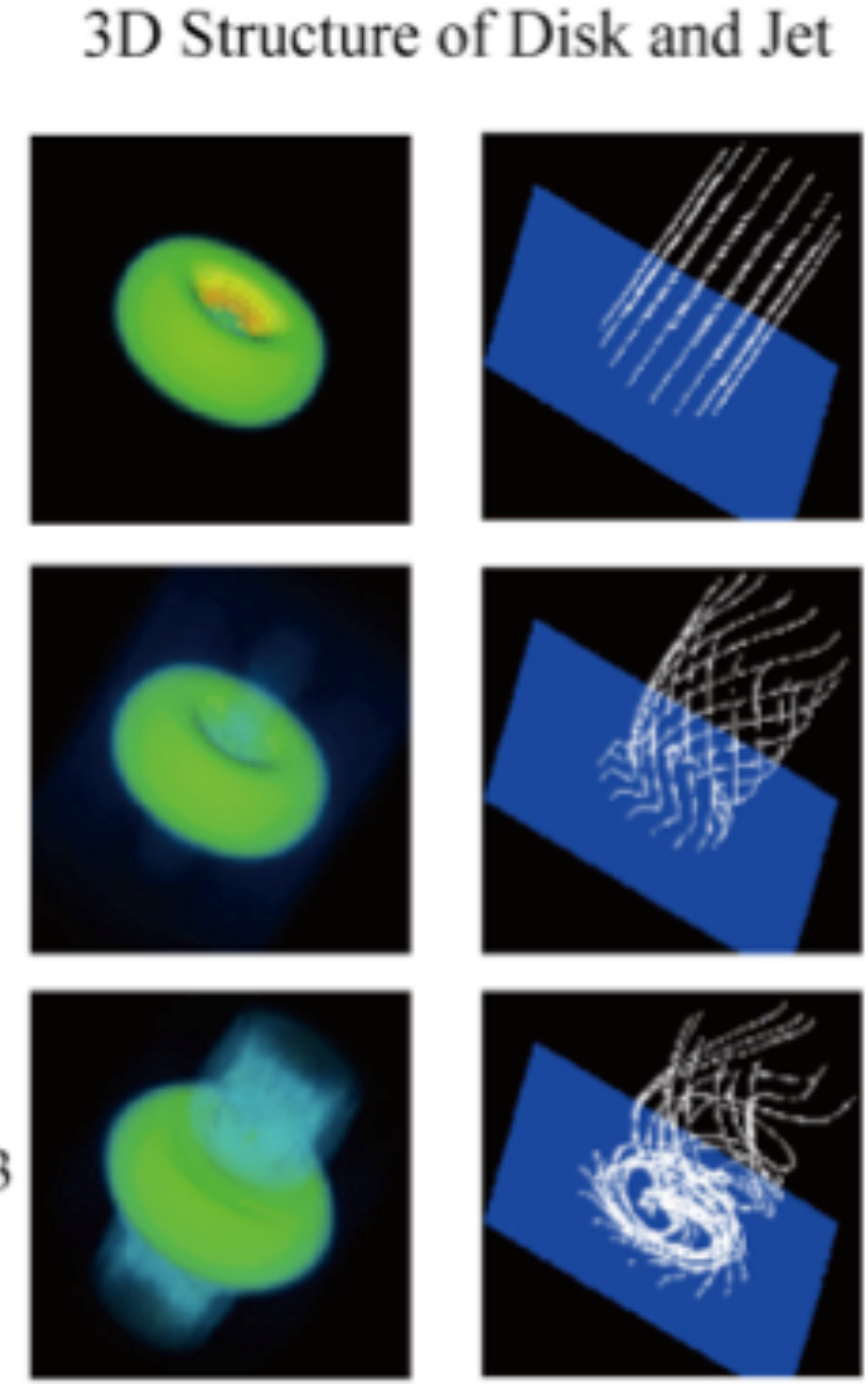

Textbook p. 387

Magneto-Rotational Instability (MRI)

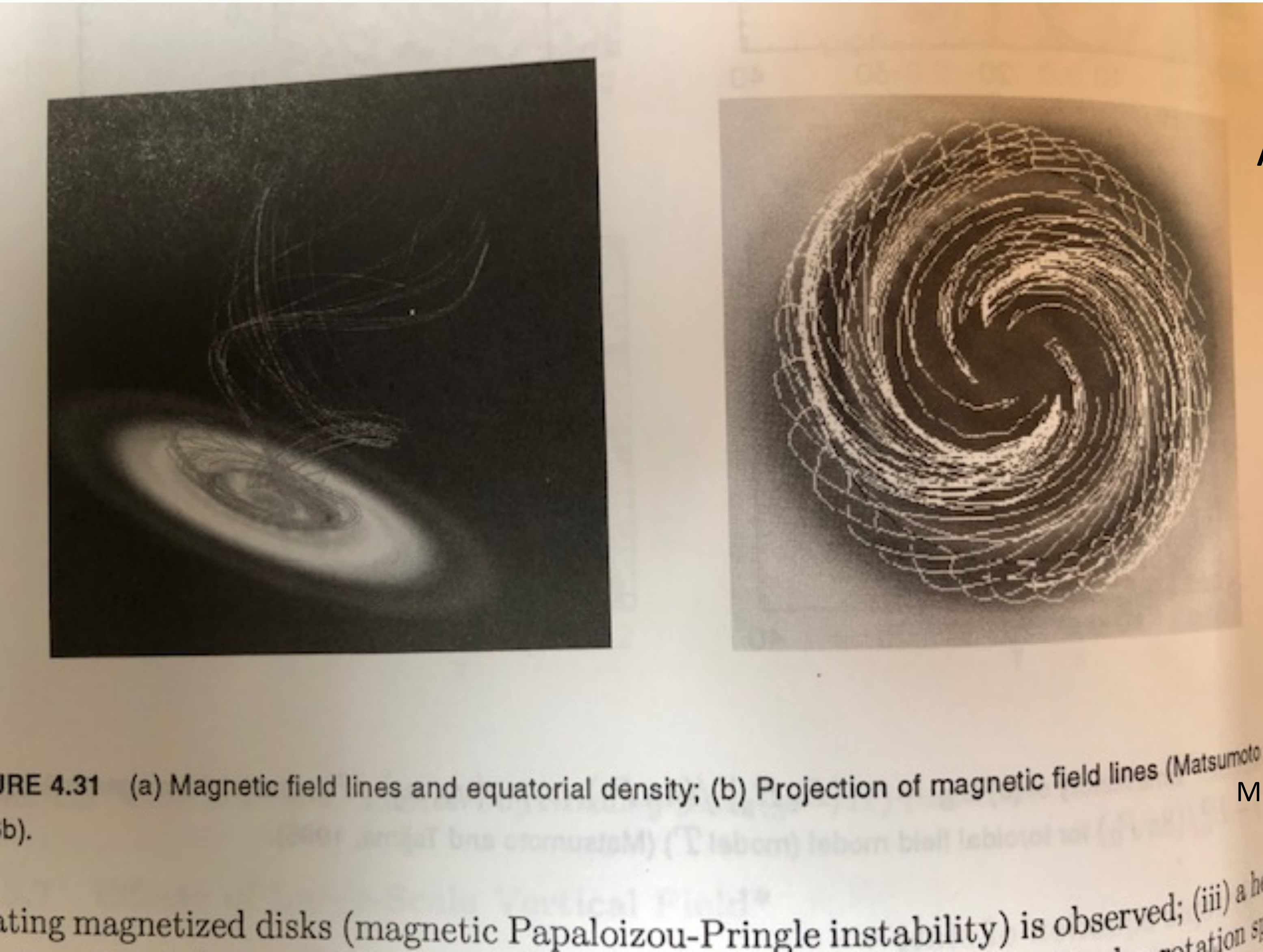

Accretion disk

rotating plasma

B-fields

(will discuss filamentary singularity)

Balbus-Hawley (1991)

Matsumoto Tajima (1995)

Text (pp.323-353)

Growth and patterns of MRI

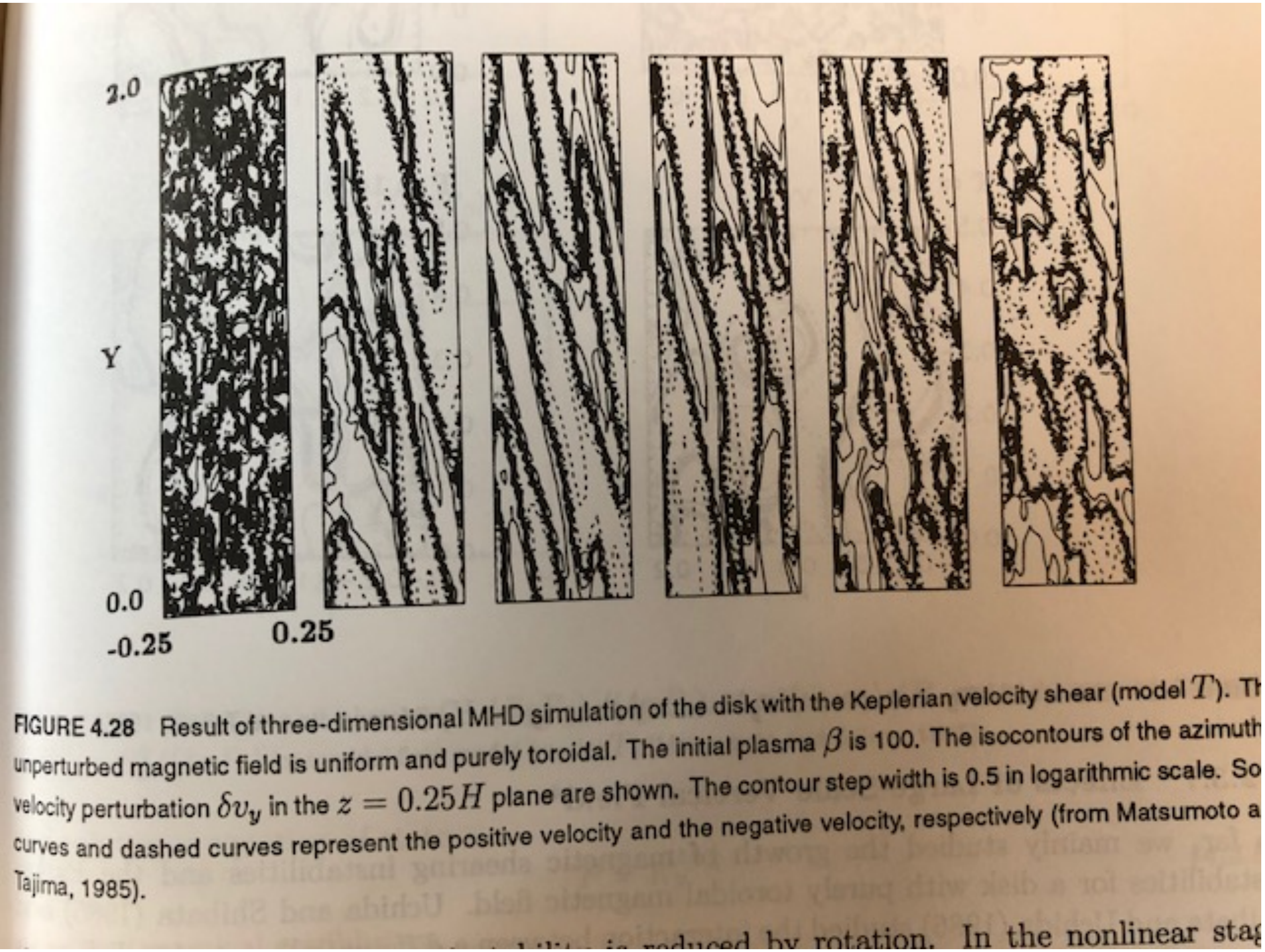

FIGURE 4.28 Result of three-dimensional MHD simulation of the disk with the Keplerian velocity shear (model T). Th
unperturbed magnetic field is uniform and purely toroidal. The initial plasma β is 100. The isocontours of the azimuth
velocity perturbation δv_y in the $z = 0.25H$ plane are shown. The contour step width is 0.5 in logarithmic scale. So
curves and dashed curves represent the positive velocity and the negative velocity, respectively (from Matsumoto a
Tajima, 1985).

reduced by rotation. In the nonlinear stag

Accretion plasma flow patterns:

← θ-r plane : δv_θ–pattern

↓

Fluctuations: Magnetic ($\delta\boldsymbol{B}$)
+ plasma velocity ($\delta\boldsymbol{v}$)

↓

Enhanced transport = anomalous viscosity η

Next page: coupled equations for $\delta\boldsymbol{v}$, $\delta\boldsymbol{B}$ → 2nd order ordinary diff. eq. in radial dir.

→ analytical and physical solutions (even though there is an Alfven singularity exists) found

4.2.3.2 Alfvén Singularities and Eigenmodes*

In this subsection we derive the wave equation in differentially rotating magnetized disks and solve the eigenvalue problem. In the unperturbed state, the density, pressure, and magnetic fields are assumed to be uniform. By assuming that $v_x = v_z = 0$ in the unperturbed state, the unperturbed momentum equation is

$$g + 2v_0 \times \Omega + (\Omega \times r) \times \Omega = 0. \qquad (4.2.49)$$

We further assume that $B_x = 0$ in the unperturbed state. We linearize the basic equations and look for eigenmode solutions of the form $\tilde{\phi}(x,t)\exp[i(k_y y + k_z z)]$ according to the above discussion. The Laplace transform of the momentum equation and the induction equation are

plasma

$$-i\omega_d \tilde{v} - 2A\tilde{v}_x \hat{y} - 2\tilde{v} \times \Omega - \frac{(B\nabla)\tilde{b}}{4\pi\rho} + \nabla\left(\frac{B\tilde{b}}{4\pi\rho} + \frac{\delta p}{\rho}\right) - \nu\nabla^2\tilde{v} = \tilde{v}(x,0), \qquad (4.2.50)$$

and

B

$$-i\omega_d \tilde{b} + 2A\tilde{b}_x \hat{y} - (B\nabla)\tilde{v} - \eta\nabla^2\tilde{b} = \tilde{b}(x,0), \qquad (4.2.51)$$

where

$$\omega_d = \omega + 2Ak_y x \qquad (4.2.52)$$

is the Doppler shifted frequency, $\tilde{b}$, $\tilde{v}$, and δp are Laplace transform of the magnetic field, velocity, and the pressure perturbations, respectively.

Substituting these results into the Laplace transform of the continuity equation $\nabla \cdot v = 0$ yields the initial value equation

$$\omega_\eta^2 \omega_{\nu\eta}^4 \frac{d^2\tilde{v}_x}{dx^2} + 4A\omega_A^2 k_y \omega_d \omega_{\nu\eta}^2 \frac{d\tilde{v}_x}{dx} + \left[-(k_y^2 + k_z^2)\omega_\eta^2\omega_{\nu\eta}^4 - 8A^2k_y^2\omega_A^2\omega_{\nu\eta}^2 + \kappa^2 k_z^2 \omega_\eta^2(\omega_\eta^2 + A\omega_A^2/\Omega_B)\right]\tilde{v}_x = \Gamma(x,\omega) \qquad (4.2.53)$$

where

$$\omega_\eta = \omega_d + i\eta\left(k_y^2 + k_z^2 - \frac{d^2}{dx^2}\right), \qquad (4.2.54)$$

$$\omega_\nu = \omega_d + i\nu\left(k_y^2 + k_z^2 - \frac{d^2}{dx^2}\right), \qquad (4.2.55)$$

and

$$\omega_{\nu\eta}^2 = \omega_\nu\omega_\eta - \omega_A^2. \qquad (4.2.56)$$

Here $\Omega_B = \Omega - A$, $\kappa = 2(\Omega\Omega_B)^{1/2}$ is the *epicyclic frequency*, and ω_A is the Alfvén frequency

$$\omega_A^2 = \frac{(k \cdot B)^2}{4\pi\rho} = k_y^2 v_A^2. \qquad (4.2.57)$$

Alfven singularity

332

The initial condition enters through the right-hand side of Eq. (4.2.53).

First, we consider the case when there is no dissipation ($\eta = \nu = 0$). The homogeneous part of Eq. (4.2.53) reduces to the second order differential equation as

$$\frac{d^2\tilde{v}_x}{dx^2} + \frac{4A\omega_A^2 k_y}{\omega_d(\omega_d^2 - \omega_A^2)}\frac{d\tilde{v}_x}{dx} + \left[-(k_y^2 + k_z^2) - \frac{8A^2k_y^2\omega_A^2}{\omega_d^2(\omega_d^2 - \omega_A^2)} + \kappa^2 k_z^2 \frac{\omega_d^2 + A\omega_A^2/\Omega_B}{(\omega_d^2 - \omega_A^2)^2}\right]\tilde{v}_x = 0. \qquad (4.2.58)$$

Eigenfunction w/ singularity

It is noted that in the presence of shear flows the eigenmode equation such as Eq. (4.2.58) does not take the self-adjoint form anymore. This is in contrast to the standard MHD problem without shear flows, which has the *self-adjoint form* (Bernstein et al., 1958). Note that although this can be formally changed to self-adjoint form (4.2.58) must not be converted into the self-adjoint form since it includes singular terms (Arfken and Weber, 1995, p. 539). Thus the eigenvalues ω are not guaranteed to be real or pure imaginary. We express Eq. (4.2.58) in terms of

$$\xi = \frac{2Ak_y x}{\omega_A} \qquad (4.2.59)$$

as

$$\frac{d^2\tilde{v}_x}{d\xi^2} + \frac{2\omega_A^3}{\omega_d(\omega_d^2 - \omega_A^2)}\frac{d\tilde{v}_x}{d\xi} + \left[-\left(1 + \frac{1}{q}\right)\left(\frac{\omega_A}{2A}\right)^2 - \frac{2\omega_A^4}{\omega_d^2(\omega_d^2 - \omega_A^2)} + \left(\frac{\kappa}{2A}\right)^2\left(\frac{\omega_A^2}{q}\right)\frac{\omega_d^2 + A\omega_A^2/\Omega_B}{(\omega_d^2 - \omega_A^2)^2}\right]\tilde{v}_x = 0, \qquad (4.2.60)$$

where

$$q = \frac{k_z^2}{k_y^2}. \qquad (4.2.61)$$

This differential Eq. (4.2.60) has two singularities at $\omega_d = \pm\omega_A$. These are the shear Alfvén singularities where the absorption and mode conversion of Alfvén waves take place (e.g. Ross et al., 1982). The locations of Alfvén singularities in the complex plane are

$$\xi_A = \pm 1 - \frac{\omega}{\omega_A}. \qquad (4.2.62)$$

By applying the *Frobenius method* around $\omega_d = \pm\omega_A$ (or $\xi = \xi_A$), and solving the indicial equation, we find that the exponent s in the series expansion

$$\tilde{v}_x(\xi) = \sum_{n=0}^{\infty} a_n(\xi - \xi_A)^{n+s}$$

becomes complex. Thus the solutions which pass through these points are singular (called *regular singular points*). The *corotation point* $\omega_d = 0$ (or $\xi = -\omega/\omega_A$) appears to be also singular in Eq. (4.2.60). However, by solving the indicial equation, we find that the solution is regular at the corotation point.

The solutions of Eq. (4.2.60) which vanish as $\xi \to \pm\infty$ have an asymptotic form

$$\tilde{v}_x \propto \exp[\mp(1 + 1/q)^{1/2}\omega_A\xi/(2A)]. \qquad (4.2.63)$$

333

Frobenius' method

index s

degree of singularity

→ Nature of filamentary singularity

For those aficianados of math physics, enjoy the math of regular singular point eigen functions (see: Matsumoto-Tajima, Ap. J. 1995)

Solution by Frobenius Method to the MRI eigenfunction

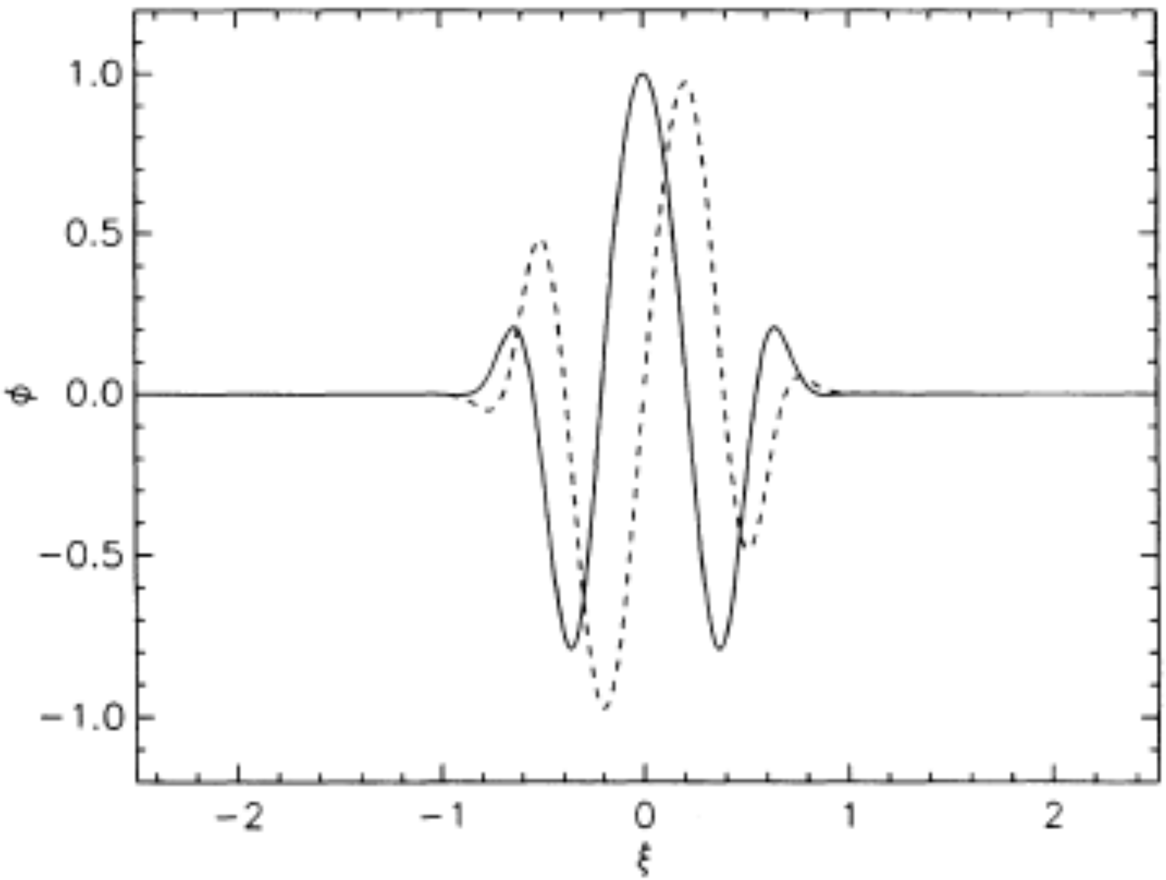

Eigenfunction amplitude

Shear flow in the azimuthal θ direction →
amplitude oscillations in r (or ξ)

FIG. 1*b* Normalized radial position ξ=0 is Alfven singularity

$$\eta = \left(\frac{\pi}{2}\right)^{1/2} \frac{1}{4\pi n_e m C_s}\left(\frac{k_y^2}{k^3}\right)_{\max}\langle\delta B^2\rangle, \tag{4.2.71}$$

where $(k_y^2/k^3)_{\max}$ is evaluated at $\mathbf{k}=\mathbf{k}_{\max}$.

Since magnetic fields induced by the magnetorotational instability eventually dominate over seed magnetic fields, we equate B^2 to $\langle\delta B^2\rangle$ to evaluate the saturation level. The saturation level of magnetic fluctuations can be determined by equating the growth rate γ of the instability with the anomalous resistivity damping ηk^2. By using Eq. (4.2.64) for γ and Eq. (4.2.71) for η, we obtain

$$\frac{\langle\delta B^2\rangle}{4\pi n_e m C_s^2} = \chi_e \left(\frac{2}{\pi}\right)\left(\frac{k^2 k_z^2}{k_y^4}\right)\left(\frac{k_\parallel^2}{k_z^2}\right) f(q), \tag{4.2.72}$$

where $\chi_e = n_e/n$ is the ionization rate. The factor $k_\parallel^2/k_z^2$ is unity for purely poloidal field. For cases with a purely toroidal field $k_\parallel^2/k_z^2 = q$. In the marginally stable state $k_\parallel^2/k_z^2$ is between q and 1 because the magnetic fields are already perturbed.

As the disk plasma is close to the marginality, the *magnetic viscosity parameter* $\alpha_B = -\langle\delta B_x \delta B_y\rangle/(4\pi\rho C_s^2)$ may be approximately written (Matsumoto and Tajima, 1995) by using the linearized momentum equation [Eq. (4.2.50)] and linearized induction equation [Eq. (4.2.51)] with $\eta = \nu = 0$ as

$$\alpha_B = \chi_e \frac{\langle\delta B^2\rangle}{4\pi n_e m C_s^2} \frac{-\left\langle \frac{\delta B_y}{\delta B_x}\right\rangle}{\left\langle\left(\frac{\delta B_y}{\delta B_x}\right)^2\right\rangle + \left\langle\left(\frac{\delta B_z}{\delta B_x}\right)^2\right\rangle + 1}, \tag{4.2.73}$$

where

$$\left\langle\frac{\delta B_y}{\delta B_x}\right\rangle = \frac{-2\Omega\gamma + (\gamma^2+\omega_A^2-4A\Omega)(k_y/k_z)}{\gamma^2+\omega_A^2+2\Omega\gamma(k_y/k_z)}, \tag{4.2.74}$$

and

$$\left\langle\frac{\delta B_z}{\delta B_x}\right\rangle = -q^{1/2}\frac{(\gamma^2+\omega_A^2)(k_z/k_y + k_y/k_z + 2A/\gamma)}{\gamma^2+\omega_A^2+2\Omega\gamma(k_y/k_z)}. \tag{4.2.75}$$

When deriving these equations, we replaced d/dx by ik_x. The notations $\langle\delta B_x \delta B_y\rangle$ etc. denote the spatial average.

The instability-induced velocity fields also contribute to the radial *angular momentum transport*. The viscosity parameter corresponding to the *Reynolds* stress $\rho\langle v_x v_y\rangle$ due to this instability is expressed (Matsumoto and Tajima, 1995) as

$$\alpha_v = \frac{\langle v_x v_y\rangle}{C_s^2} = -\alpha_B\left(\frac{\gamma^2}{\omega_A^2}\right)\frac{\langle v_y/v_x\rangle}{\langle\delta B_y/\delta B_x\rangle}, \tag{4.2.76}$$

where

$$\left\langle\frac{v_y}{v_x}\right\rangle = \left\langle\frac{\delta B_y}{\delta B_x}\right\rangle + \frac{2A}{\gamma}. \tag{4.2.77}$$

Anomalous viscosity in accretion disk

Anomalous viscosity $\eta \sim \delta B^2$
$\sim O(\alpha_B)$

$\delta v^2 \sim O(\alpha_v)$

where $\alpha_B \sim (\delta v_A / C_s)^2$
$\alpha_v \sim (\delta v / C_s)^2$

General structure of
anomalous transport

Here we set the classical
viscosity $\nu=0$ and resistivity $\eta=0$

Typical astronomical *observed* and
our *simulational* values of
$\alpha \sim 0.1$

Evolution of accretion disks

- Anomalous viscosity → "**growth hormone**"
  of the AGN (young galaxies), $0 < \alpha < 1$
  stars, Universe in general
- Feeder of matter / energy to AGN and jets
  brightening and growth of AGN, jets

→ Fundamentals for evolution of the Universe

Episodic transitions of accretion disks with B

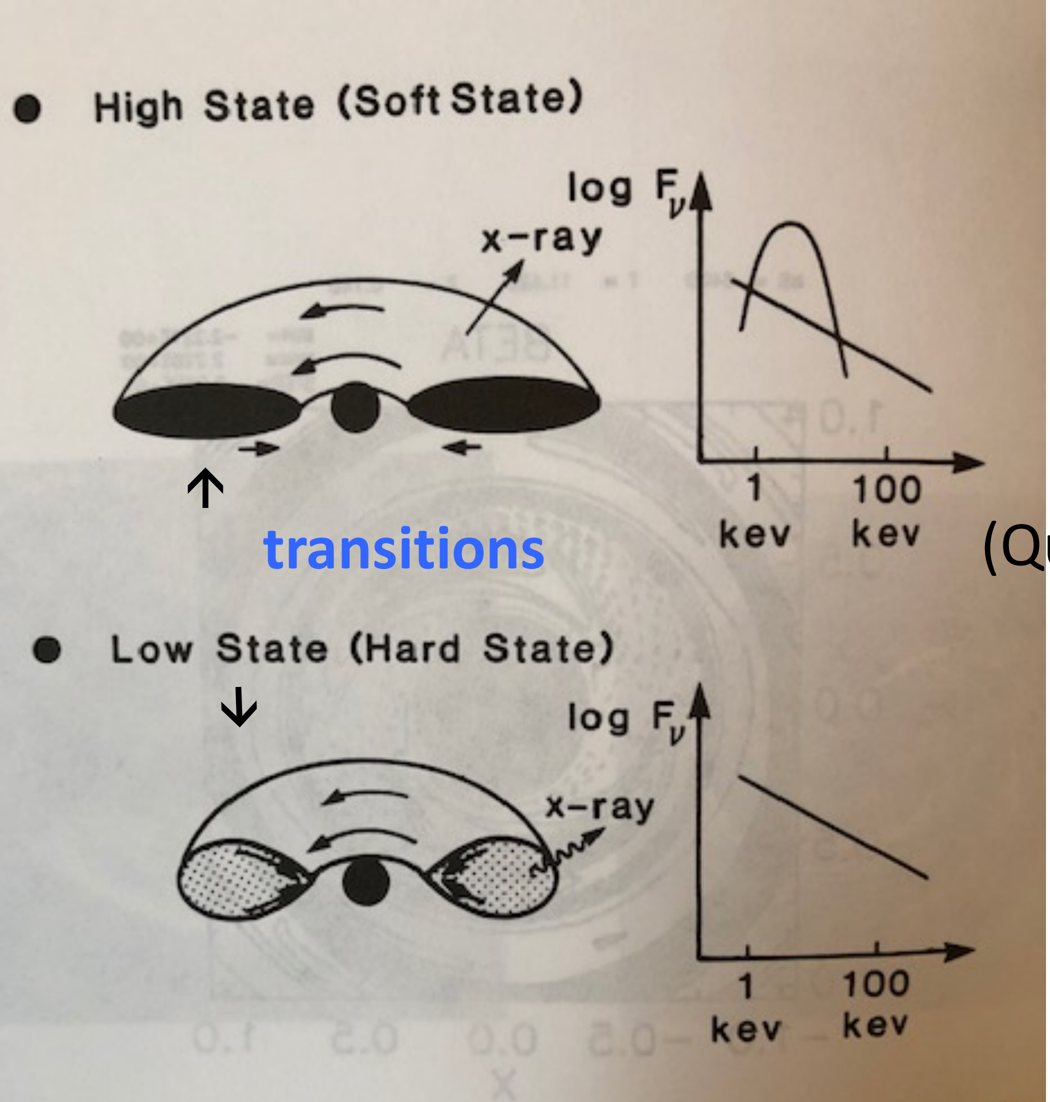

3 Two states of accretion disks: "High state" (soft state) vs. "Low state" (hard state): the
ectra

nown that accretion disks in black hole candidates have two spectral state
n, 1984). One is the high state and the other is the low state. In the hi
spectra has blackbody component which can be explained by emission
k accretion disks. On the other hand, in the low (or hard) state, the sp
law which may come from optically thin accretion disk (Fig. 4.33). Other

(Quasi-)steady state accretion disks

cf.

Episodic accretion disks

"breathing" disks

transitions between the **states**

soft state (β >>1)

↑↓

hard state (β ~ 1)